JOURNAL OF MATERIALS SCIENCE **34** (1999) 2139–2149

Three-dimensional elastoplastic finite element modelling of deformation and fracture behaviour of rubber-modified polycarbonates at different triaxiality

XIAO-HONG CHEN, YIU-WING MAI
Centre for Advanced Materials Technology (CAMT), Department of Mechanical & Mechatronic Engineering J07, The University of Sydney, Sydney, NSW 2006, Australia
E-mail: mai@mech.eng.usyd.edu.au

A periodic face-centred cuboidal cell model is provided to account for inter-particle interaction, and a particle-crack tip interaction model is developed to study the interaction between a blunting model I crack tip and the closest array of initially spherical rubber particles in an effective medium. Three-dimensional elastoplastic finite element analysis has been preformed to study the deformation and fracture behaviour of rubber-modified polycarbonates. The effective elastoplastic constitutive relation is derived by the method of homogenisation and local stress and strain distributions are obtained to explore the role of rubber cavitation in the toughening process at different stress triaxiality. 3D elastoplastic finite element results are compatible with experimental observations, that is, rubber particles can act as stress concentrators to initiate crazing or shear yielding in the matrix but they behave differently from voids at high triaxiality. Rubber cavitation plays an important role in the toughening process under high tensile triaxial stresses. © *1999 Kluwer Academic Publishers*

1. Introduction

Rubber modification has been widely used to enhance the fracture toughness of many brittle and semi-brittle polymers. Over the past few years, understanding of various toughening mechanisms in rubber-modified polymers has been advanced by extensive experimental and analytical work [1–4]. Rubber cavitation, matrix crazing and shear yielding have been identified as three major toughening mechanisms. The significance of rubber cavitation and the sequence of the associated toughening mechanisms have been the subject of many previous studies. The departure of theoretical prediction from experimental observation is mainly caused by the inaccurate modelling of crack tip constraint and/or loading conditions.

Yee and coworkers [5, 6] and Wu and Mai [7] reported direct experimental evidence of constraint relief due to rubber cavitation in the high triaxial tension region associated with a crack tip for extensive matrix shear yielding to occur in rubber-modified epoxies and polycarbonates. It is shown that rubber cavitation occurs first, followed by massive shear yielding of the matrix material. Sue and Yee [8] studied the tensile behaviour of a polycarbonate plate with a circular hole by 2D finite element analysis and experimental observation. It is shown that the maximum octahedral shear stress is shifted around the interface from the equator of particles towards the $\pm 45^\circ$ region as the applied tensile stress is increased. Huang and Kinloch [9] developed a 2D plane-strain periodic cell model with one particle surrounded by four neighbouring particles in a staggered layout to demonstrate successfully the localised shear banding process but *not* the rubber cavitational process because they used a low rubber bulk modulus and dealt with a simple tension case. Schemer *et al.* [10] simulated the deformation and cavitational process in rubber-toughened polycarbonate by 2D plane-strain finite element analysis. However, since polycarbonate specimens tend to undergo brittle fracture under a high tensile triaxial stress state associated with a macrocrack, these 2D finite element analyses are difficult to be extended to the real case of a crack in a thick rubber-modified PC specimen due to the differences in constraint/loading conditions.

Guild and Kinloch [11] developed a periodic spherical cell model to investigate the stress and strain distributions in rubber-modified epoxies under triaxial stress state using axisymmetric elastic and elastic-plastic finite element analyses. The spherical model is based on the assumption that the overall effect of inter-particle interaction for random distribution is an 'average' from all the neighbouring particles and not directional, which leads to an underestimation of the inter-particle interaction. Moreover, it is not easy to use this method to model the real crack-tip stress and strain fields because it is confined to axisymmetric conditions. Sue

and Yee [12] conducted a micromechanical investigation on the spherical rubber particle cavitational process near a crack tip using a combination of Irwin's crack-tip analysis, slip-line field theory and Dewey's closed-form elastic solution. The stresses in front of a crack-tip elastic-plastic boundary were used as the farfield boundary conditions to calculate the local stress concentrations around a spherical rubber particle or void in the case that both particle-particle and particle-crack tip interactions can be neglected. It is assumed that the inclusion size is much smaller than the sizes of the crack and its corresponding plastic zone and also the inclusion is located just outside the crack-tip plastic zone where Dewey's solution still applies.

Chen and Mai [13, 14] provided a face-centred cuboidal (FCC) cell model to study the toughening mechanisms in rubber-modified epoxies using 3D elastoplastic FEA because it is easy to simulate both rubber cavitation and matrix shear banding processes using such a staggered periodic layout, which includes the full inter-particle interaction and removes the axisymmetric requirement. Wu, Wu and Mai [15, 16] carried out 2D plane-strain elastoplastic finite element analysis to study the effects of volume fraction and bulk modulus of rubber particles on toughening mechanisms for rubber-modified epoxies with a pre-existing macrocrack. Hom and McMeeking [17, 18] pointed out in their study on void growth near a mode I plane-strain crack tip that the coupling effects may be stronger in 2D problems for cylindrical holes than in 3D problems for initially spherical voids. But they did not study the rubber toughening mechanisms.

In this paper, three-dimensional elastoplastic finite element analysis is carried out to obtain the local stress and strain fields for rubber-toughened polycarbonates under various constraint/loading conditions. A 3D periodic face-centred cuboidal (FCC) cell model is adopted to describe the distribution of rubber particles in the PC matrix. A 3D particle-crack tip interaction model is provided to study the interaction between a blunting mode I crack tip and the closest array of initially spherical rubber particles located parallel to and directly ahead of the crack front in the effective medium. Other interactions are taken into account through the effective stress-strain relation for the effective medium obtained from the face-centred cuboidal (FCC) cell model.

2. 3D micromechanical modelling

Because a 3D crack problem is both complex and time-consuming, we have to make some simplifications in order to carry out 3D elastoplastic finite element analysis. Two different ways will be adopted to examine the toughening process in rubber-modified polycarbonates with a face-centred cubic layout, as shown in Fig. 1. The matrix is assumed to be elastic-plastic governed by the Von Mises criterion and the particles isotropic elastic. First, we will study the local stress and strain fields in a periodic face-centred cuboidal cell subjected to uniaxial tension and prescribed stress systems in front of the crack-tip elastic-plastic boundary. Then we will consider the interaction of a blunting mode I plane-strain crack tip with the closest periodic array of initially spherical rubber particles located directly ahead of and parallel to the crack front in the effective medium by a sub-modelling technique.

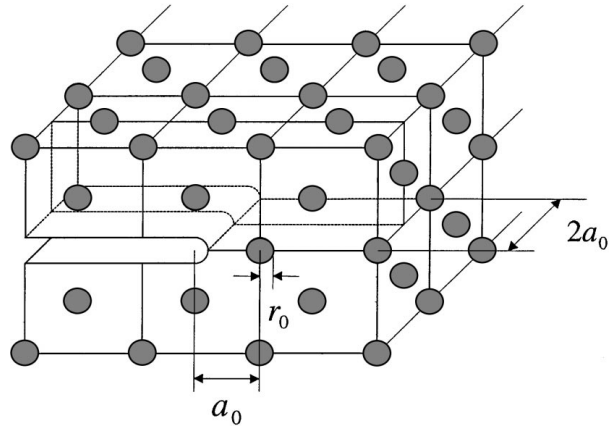

Figure 1 A plane-strain crack in rubber-modified polymers with a face-centred cubic layout.

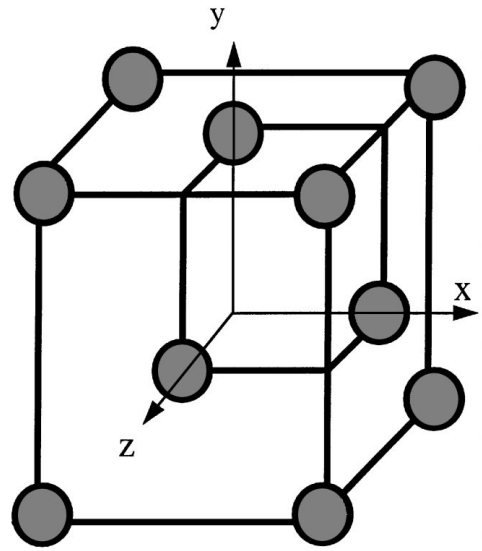

Figure 2 Face-centred cuboidal cell model.

2.1. Face-centred cuboidal cell model

The representative unit of the periodic FCC microstructure is shown in Fig. 2. Under symmetric loading condition, a one-eighth face-centred cuboidal cell can be chosen due to the periodic symmetry of the problem.

The periodic symmetry requirements are satisfied by imposing the following constraint equations on the corresponding surfaces of the cell

$$\begin{aligned} u_x &= U_{x0}, \quad t_y = t_z = 0 \quad \text{at } x = a_0 \\ u_y &= U_{y0}, \quad t_x = t_z = 0 \quad \text{at } y = a_0 \\ u_z &= U_{z0}, \quad t_x = t_y = 0 \quad \text{at } z = a_0 \end{aligned} \tag{1}$$

and

$$\begin{aligned} u_x &= 0, \quad t_y = t_z = 0 \quad \text{at } x = 0 \\ u_y &= 0, \quad t_x = t_z = 0 \quad \text{at } y = 0 \\ u_z &= 0, \quad t_x = t_y = 0 \quad \text{at } z = 0 \end{aligned} \tag{2}$$

where a_0 is the cell length, (u_x, u_y, u_z) and (t_x, t_y, t_z) are the components of displacement vector **u** and surface traction vector **t** along x-, y- and z- directions, U_{x0}, U_{y0} and U_{z0} are displacement constants. The surfaces of $x = a_0$, $y = a_0$ and $z = a_0$ are kept parallel with respect

to their original shapes during deformation to satisfy the periodic symmetry requirements.

The effective stress $\boldsymbol{\sigma}^{\mathrm{e}}$ and strain $\boldsymbol{\varepsilon}^{\mathrm{e}}$ are obtained by averaging the local stress $\boldsymbol{\sigma}$ and strain $\boldsymbol{\varepsilon}$ in the cell, that is,

$$\boldsymbol{\sigma}^{\mathrm{e}} = \frac{1}{V_\Omega}\int_{V_\Omega} \boldsymbol{\sigma}\,\mathrm{d}V = \frac{1}{V_\Omega}\int_{S_\Omega} \mathbf{r}\otimes\mathbf{t}\,\mathrm{d}S \qquad (3)$$

$$\boldsymbol{\varepsilon}^{\mathrm{e}} = \frac{1}{V_\Omega}\int_{V_\Omega} \boldsymbol{\varepsilon}\,\mathrm{d}V = \boldsymbol{\varepsilon}^{0} \qquad (4)$$

where $\mathbf{r}$ is the position vector, $\boldsymbol{\varepsilon}^0$ is the constant strain tensor dependent on the constant normal displacement on the cell surface, V_Ω and S_Ω represent the cell volume and surface, respectively. We use the equilibrium condition without volume force, i.e. $\nabla\cdot\boldsymbol{\sigma} = 0$, to obtain the last equality of (3). We can ensure the desired level of effective true stress system without axisymmetric requirement by adjusting the uniform normal displacement increment of each face of the unit cell [13, 14, 17, 18].

2.2. Particle-crack tip interaction model

The solution of a 3D crack problem is possibly periodic only along the crack front direction but not periodic in the perpendicular plane. We cannot model many rubber particles with the crack simultaneously due to the large storage capacity and computation efficiency required for such a 3D crack problem. For simplification of numerical analysis, we consider the interaction of a blunting model I crack tip with the closest periodic array of initially spherical rubber particles located directly ahead of and parallel to the crack front in the effective medium with other interactions taken into account through the effective stress-strain relation for the effective medium obtained in Section 2.1 using a face-centred cuboidal cell model. Following the methods by Wu *et al.* [15, 16] and Hom and McMeeking [17, 18], the blunting crack tip has an initial notch radius of r_0 equal to the radius of rubber particles. Rubber particles are equidistant from the notch center with an initial distance a_0 and evenly spaced from each other with an initial distance $2a_0$ in the crack front direction. We change the initial distance a_0 from $5r_0$ to $2.5r_0$ while keeping the particle size constant, which gives a particle volume fraction of 1.68% and 13.40%, respectively (i.e., $f_{\mathrm{r}} = 2\pi r_0^3/3a^3$). Owing to the periodicity in the crack front direction and the symmetry with the crack plane of the problem, a domain extending one-half wavelength of the periodic array above the crack plane is considered for analysis, as shown in Fig. 3. The y-axis is perpendicular to the crack plane and the z-axis is parallel to the crack front.

The normal displacement and shear forces on the symmetry and periodic symmetry planes should be zero. These requirements are satisfied by imposing the following constraint equations:

$$u_y = 0 \quad t_x = t_z = 0 \qquad \text{at } y = 0 \text{ (symmetry)} \qquad (5)$$

$$u_z = 0 \quad t_x = t_y = 0 \qquad \text{at } z = 0 \quad \text{and} \quad z = a_0 \text{ (periodic symmetry)} \qquad (6)$$

and the crack surface is traction free.

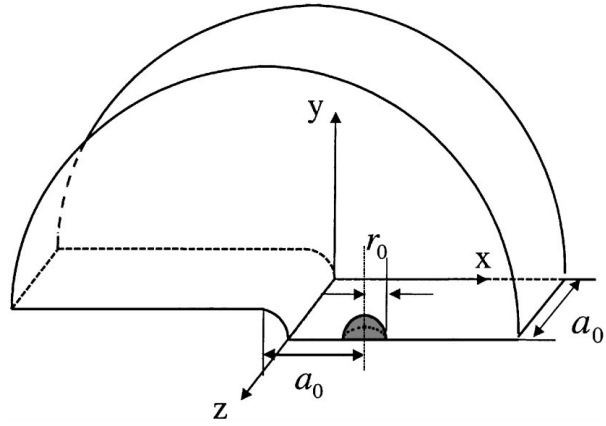

Figure 3 Particle-crack tip interaction model.

The asymptotic displacement field for the mode I plane-strain crack tip by LEFM is used as the outer boundary condition under small-scale yielding condition

$$u_x = \frac{K_{\mathrm{I}}}{E^{\mathrm{e}}}2(1+\nu^{\mathrm{e}}) \times \left(\frac{r}{2\pi}\right)^{1/2}\cos\frac{\theta}{2}\left[1-2\nu^{\mathrm{e}}+\sin^2\frac{\theta}{2}\right]$$

$$u_y = \frac{K_{\mathrm{I}}}{E^{\mathrm{e}}}2(1+\nu^{\mathrm{e}}) \times \left(\frac{r}{2\pi}\right)^{1/2}\sin\frac{\theta}{2}\left[2-2\nu^{\mathrm{e}}-\cos^2\frac{\theta}{2}\right] \qquad (7)$$

where r and θ are the polar coordinates, K_{I} is the mode I stress intensity factor, E^{e} is the effective Young's modulus and ν^{e} is the effective Poisson's ratio. The dimensionless stress intensity factor is defined as $\bar{K}_{\mathrm{I}} = K_{\mathrm{I}}/\sigma_{\mathrm{y}} r_0^{1/2}$, where σ_{y} is the matrix yield strength and r_0 is the initial notch radius.

Equation (5) is the symmetry condition about the crack plane, (6) is the periodic symmetry condition along the crack front direction and (7) is the outer boundary condition prescribed by the asymptotic elastic crack tip displacement solution. Periodicity for the solution of such a crack problem exists only in the z-direction and breaks down in the x- and y-directions due to the existence of a crack although the distribution of rubber particles is 3D periodic, so we can only apply the periodic condition in the z-direction to simplify the numerical analysis.

3. Three-dimensional elastoplastic finite element analysis

3.1. Effective mechanical properties by face-centred cuboidal cell model

The PATRAN program is used for automatic mesh generation. The model has a total of 17079 four-node tetrahedron elements and 4969 nodes at a particle volume fraction of 1.68%, and 8491 four-node tetrahedron elements and 1844 nodes at a particle volume fraction of 13.40%. The matrix has typical mechanical properties for polycarbonate with Young's modulus of 2400 MPa, Poisson's ratio of 0.42 and yield strength of 75 MPa

[12]. The corresponding bulk modulus for the matrix is 5000 MPa. Rubber particles have Young's modulus of 1 MPa and Poisson's ratio of 0.4999, which are within the typical range for rubber properties [4, 19]. The corresponding rubber bulk modulus is hence 1667 MPa. Three-dimensional elastoplastic finite element analysis was carried out by the ABAQUS program on ALPHA STATION 500 at the CAMT. True stress and logarithmic strain were adopted in the calculations. For comparison, we use the same mesh to do the calculations for the void/matrix system with rubber particles replaced by voids.

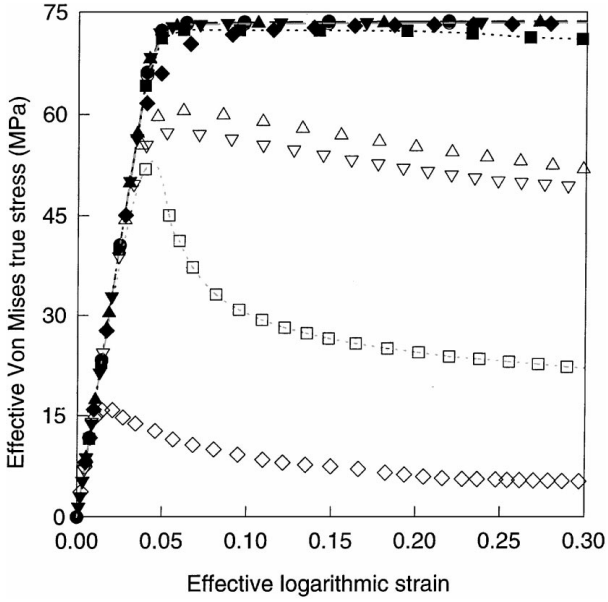

Figure 4 Effective Von Mises true stress versus effective logarithmic strain at different stress triaxiality for a particle volume fraction of 1.68%. (Solid symbols: rubber-PC. Open symbols: void-PC). —●— uniaxial tension; ---■--- uniaxial deformation; ▲ $\sigma^e_{yy}:\sigma^e_{zz}:\sigma^e_{xx}=2.5:2.0:1.5$; ▼ $\sigma^e_{yy}:\sigma^e_{zz}:\sigma^e_{xx}=2.4:1.7:1.6$; ♦ $\sigma^e_{yy}:\sigma^e_{zz}:\sigma^e_{xx}=1:0.9:0.9$.

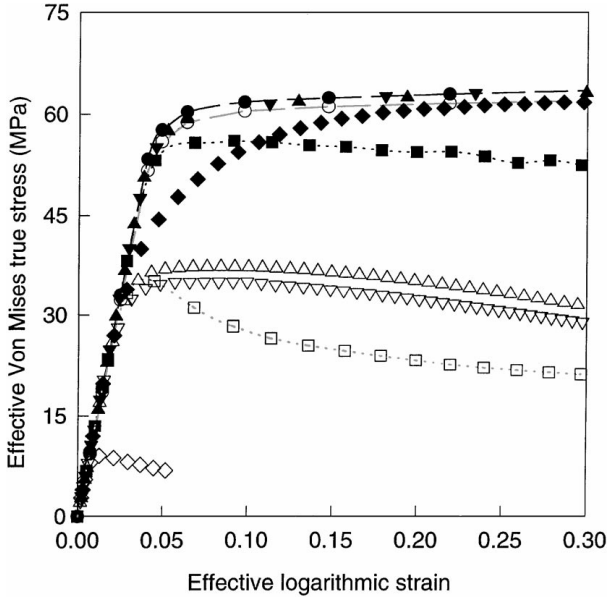

Figure 5 Effective Von Mises true stress versus effective logarithmic strain at different stress triaxiality for a particle volume fraction of 13.40%. (Solid symbols: rubber-PC. Open symbols: void-PC). —●— uniaxial tension; ---■--- uniaxial deformation; ▲ $\sigma^e_{yy}:\sigma^e_{zz}:\sigma^e_{xx}=2.5:2.0:1.5$; ▼ $\sigma^e_{yy}:\sigma^e_{zz}:\sigma^e_{xx}=2.4:1.7:1.6$; ♦ $\sigma^e_{yy}:\sigma^e_{zz}:\sigma^e_{xx}=1:0.9:0.9$.

The local stress and strain fields in the cuboidal cell are calculated for the rubber/matrix and void/matrix systems under uniaxial tension ($\sigma^e_{yy}:\sigma^e_{zz}:\sigma^e_{xx}=1:0:0$), uniaxial deformation ($\varepsilon^e_{yy}:\varepsilon^e_{zz}:\varepsilon^e_{xx}=1:0:0$) and two crack-tip stress systems ($\sigma^e_{yy}:\sigma^e_{zz}:\sigma^e_{xx}=2.5:2.0:1.5$ [20], $2.4:1.7:1.6$ [12]) as well as very high triaxiality ($\sigma^e_{yy}:\sigma^e_{zz}:\sigma^e_{xx}=1:0.9:0.9$), then the effective constitutive relation is derived by a homogenisation procedure, as shown in Figs 4 and 5 for particle volume fractions of 1.68 and 13.40%, respectively. Comparison with the Mori-Tanaka theory for the effective elastic moduli [21] is given in Fig. 6. The effective Von Mises stress is defined as $\sigma^e_s=\sqrt{3\mathbf{S}^e:\mathbf{S}^e/2}$ where $\mathbf{S}^e=\boldsymbol{\sigma}^e-\sigma^e_m\boldsymbol{I}$ is the deviatoric part of the effective stress tensor $\boldsymbol{\sigma}^e$ with the effective mean stress $\sigma^e_m=\boldsymbol{\sigma}^e:\boldsymbol{I}/3$. The effective stress triaxiality is defined as $R^e_\sigma=\sigma^e_m/\sigma^e_s$.

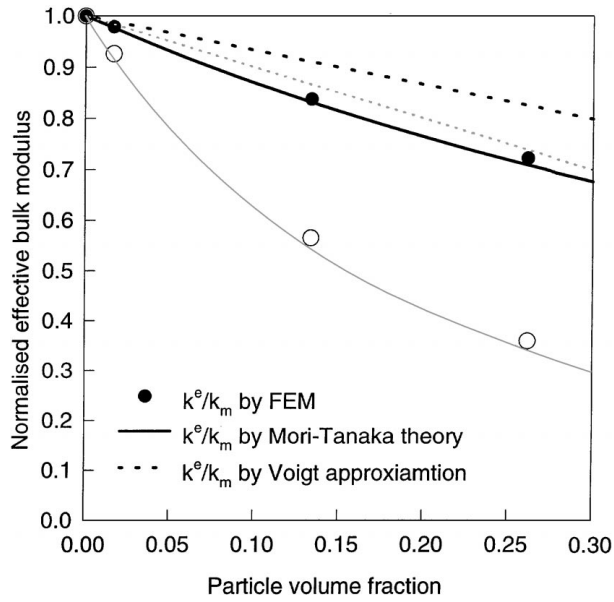

(a)

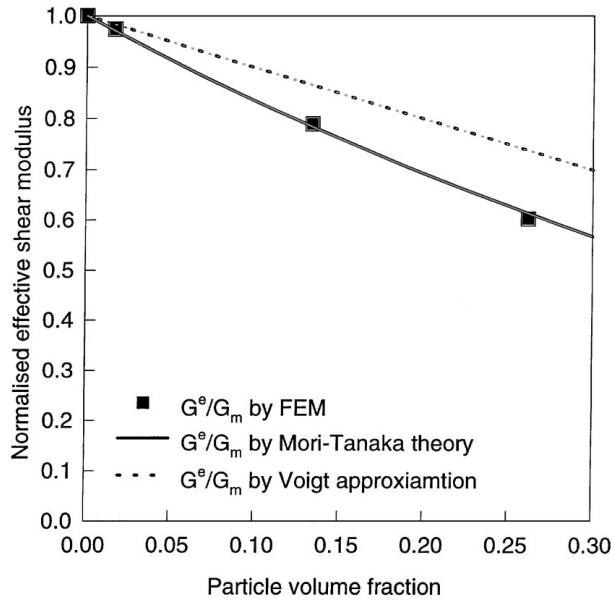

(b)

Figure 6 Dependence of effective elastic moduli on particle volume fraction. (Small solid symbol/thick black line: rubber-PC. Large open symbol/thin grey line: void-PC): (a) normalised effective bulk modulus and (b) normalised effective shear modulus.

We can see that rubber particles behave almost the same as voids under uniaxial tension but quite differently at high triaxiality. The effective stress-strain curves are lowered with increasing particle volume fraction and triaxiality. Slight strain-hardening appears for both rubber/PC and void/PC systems at low stress triaxiality. On the other hand, notable strain-hardening for rubber/PC system but strain-softening for void/PC system appears at high stress triaxiality. Effective elastic moduli decrease with increasing particle volume fraction but do not change with effective stress triaxiality. They are quite close to the predictions by the Mori-Tanaka theory compared with the Voigt upper bound. Because rubber has high bulk modulus and low shear modulus, the rubber/PC system has a much higher effective bulk modulus than the void/PC system; but they have almost the same effective shear modulus within the rubber/void concentration range we have examined. The yield point is estimated to be at the sharp reduction of the slope of the effective stress-strain curve. Effective shear yield stress is affected greatly by particle volume fraction and hydrostatic stress. At low triaxiality the effective yield stresses for rubber/PC system and void/PC system are almost the same while at high triaxiality effective yield stress drops more rapidly for the latter than for the former. The difference becomes larger with increasing particle volume fraction. At high triaxiality the rubber/PC system needs a much higher stress for the development of plastic deformation than the void/PC system. The lower yield strength and stronger inter-particle interaction at a higher particle volume fraction leads to an enhancement in shear yielding but a reduction in the load carrying capacity. As a result, there may be an optimum particle volume fraction to improve fracture toughness.

3.2. Local stress and strain fields by particle-crack tip interaction model

The effective stress-strain curve obtained for rubber-modified polycarbonates under the crack-tip stress system of $\sigma^{e}_{yy} : \sigma^{e}_{zz} : \sigma^{e}_{xx} = 2.5 : 2.0 : 1.5$ [20] is used here for the effective medium*. The PATRAN program is used to generate the mesh automatically. The interaction between the crack tip and rubber particles is modelled by mesh B, which is surrounded by mesh A with an outer radius 10 times the outer radius of mesh B, as shown in Fig. 7. These two concentric meshes of A and B for the global model and sub-model adopted in the sub-modelling technique ensure the satisfaction of the conditions of small-scale yielding as well as local disturbance due to the existence of the periodic array of rubber particles so that a detailed solution in the local region can be obtained.

We change the concentration of rubber particles by varying the inter-particle distance while keeping the particle size constant. The global model totally has 4746 six-node triangular prism elements and 3786 nodes. The sub-model totally has 16773 four-node tetrahedron elements and 3745 nodes at a particle volume fraction of 1.68%, and 19435 four-node tetrahedron elements and 4242 nodes at a particle volume fraction of 13.40%. We use the same mesh to do the calculations for the void/crack tip system with the periodic array of rubber particles replaced by the periodic array of voids.

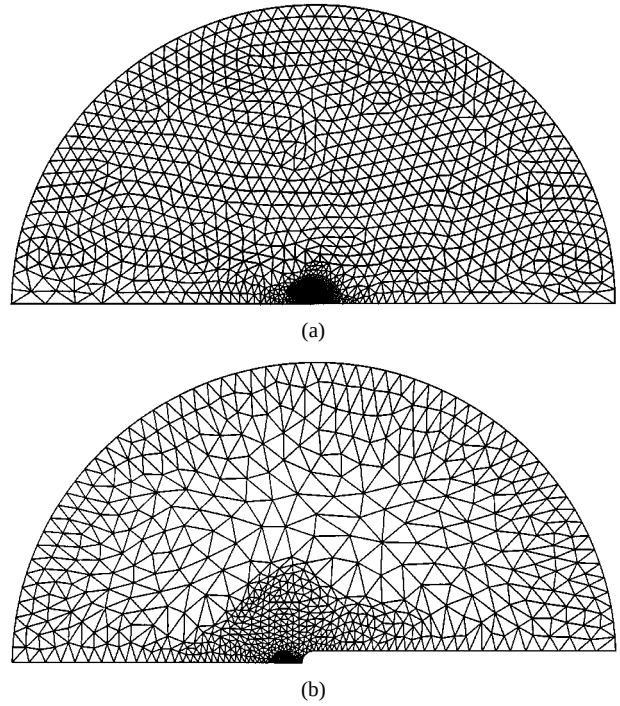

Figure 7 FEA meshes for the global model and sub-model: (a) global model and (b) sub-model.

Three-dimensional elastoplastic finite element analysis was carried out up to a dimensionless stress intensity factor $\bar{K}_{I} = 10$ with the ABAQUS program. True stress and logarithmic strain were used in the calculations. The global model is analysed first by applying the displacement condition incrementally on the outer boundary of mesh A to impose an asymptotic dependence on the mode I plane-strain elastic crack tip solution, and then the sub-model is analysed based on interpolation of the displacement solution from the global model onto the nodes at the outer boundary of mesh B with the same increment. The typical running time is 0.5 h for the global model and 2 h for the sub-model.

The contour plots of Von Mises stress in the central domain around the crack tip based on the deformed shape at different stress intensity factors for rubber/crack tip and void/crack tip systems at a particle volume fraction of 1.68% are shown in Figs 8 and 9, respectively, where the stresses are in MPa. As the crack-tip plastic zone is far away from the rubber particle/void, it will not be influenced by the existence of rubber particle/void although the shear stress distribution near the rubber particle/void undergoes some disturbance initiated by the rubber particle/void. As the crack-tip plastic zone is approaching the rubber particle/void, stress overlapping appears in the ligament between the crack tip and the rubber particle/void due to their interaction and the crack-tip plastic zone protrudes

* The stress system of $\sigma^{e}_{yy} : \sigma^{e}_{zz} : \sigma^{e}_{xx} = 2.5 : 2.0 : 1.5$ is located at the elastic-plastic boundary of the crack tip in the crack direction for which the effective stress-strain curve has been obtained. In theory the stress system along the elastic-plastic boundary will change. But in our calculation we have not considered this variation. For rubber/PC with f_r up to 13.4%, this error is minimal for the non-voided case. But the error can be large for the voided case.

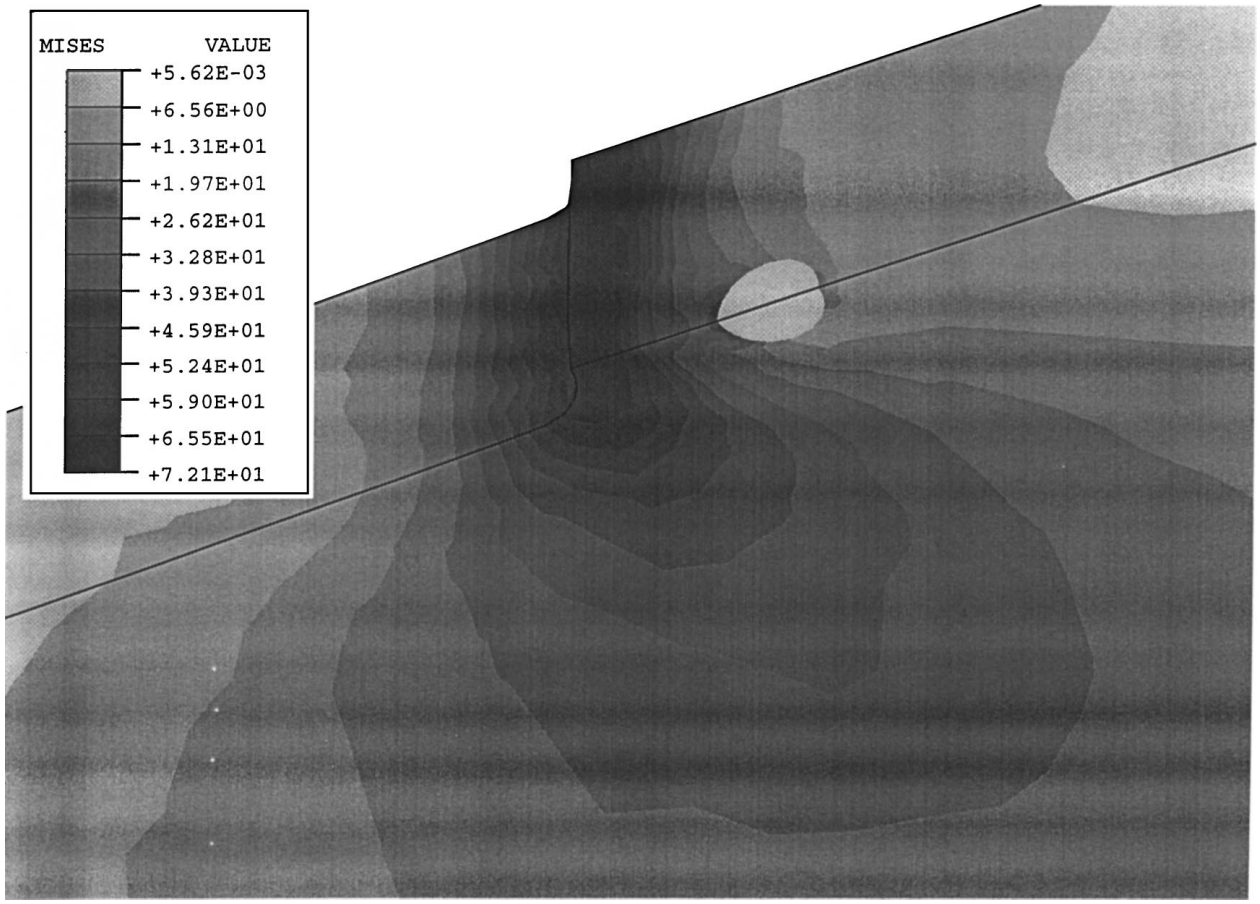

(a)

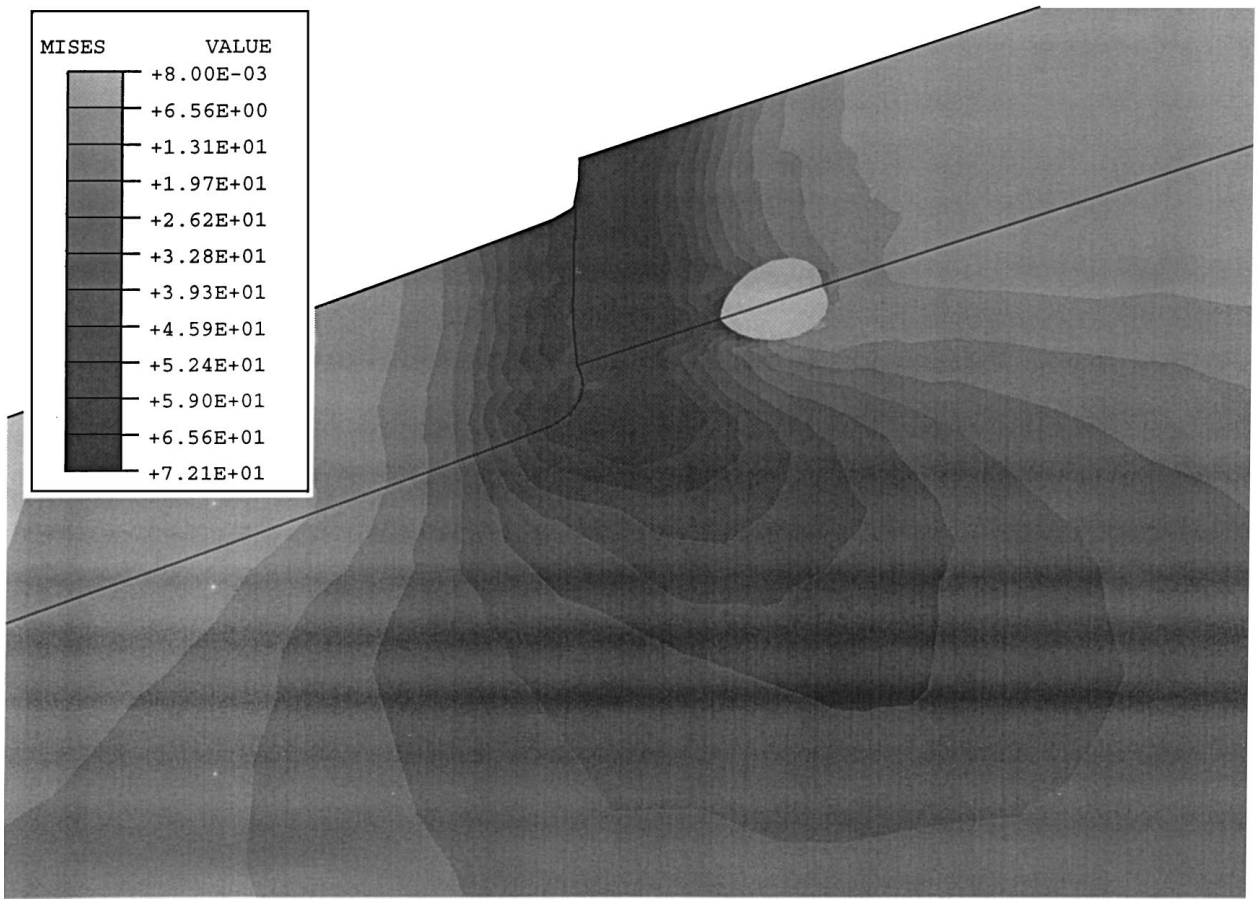

(b)

Figure 8 Contour plot of Von Mises stress in the central domain around the crack tip based on the deformed shape for rubber particle/crack tip system at a particle volume fraction of 1.68%: (a) $\bar{K}_I = 3.0$, (b) $\bar{K}_I = 3.8$, (c) $\bar{K}_I = 4.0$. (*Continued*).

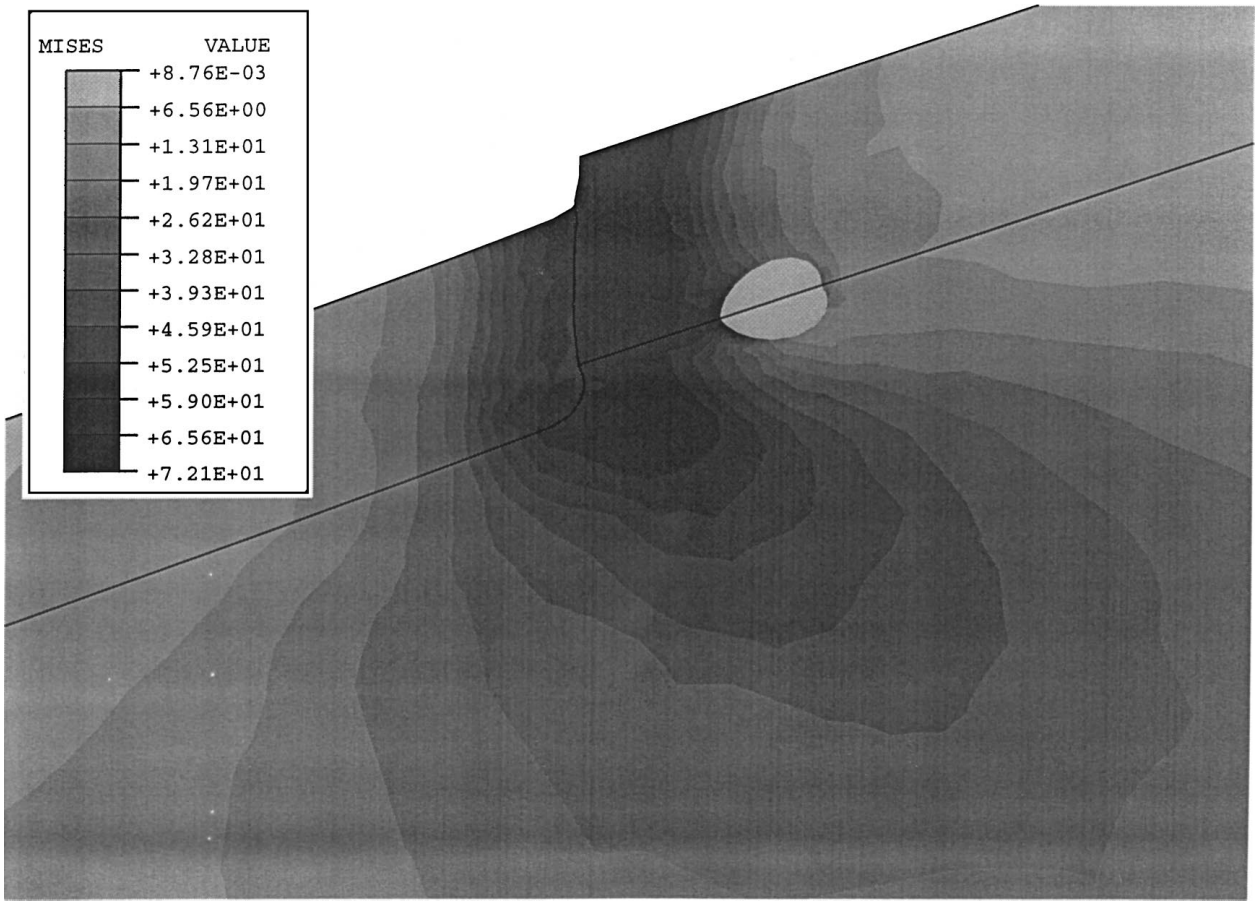

(c)

Figure 8 (*Continued*).

towards the rubber particle/void. Shear yielding occurs first in the matrix ahead of the crack tip, then in the matrix surrounding the rubber particle/void and finally the crack-tip plastic zone is connected with the plastic region surrounding the rubber particle at $\bar{K}_I = 4.0$ and the void at $\bar{K}_I$ = 3.6, respectively. Voids cause shear yielding earlier than rubber particles, which indicates that rubber cavitation is beneficial to the development of extensive shear deformation in the matrix.

The maximum octahedral shear stress, hydrostatic tension and principal stress for PC/rubber and PC/void systems under various constraint/loading conditions by the face-centred cuboidal cell model and particle-crack tip interaction model are shown in Table I in comparison with the results obtained by Sue and Yee [12]. We change the particle Poisson's ratio from 0.49 to 0.4999. The inter-particle distance a_0 is equal to five times the particle radius r_0, corresponding to a particle volume fraction of 1.68%. From the elastic analysis by Dewey's elastic solution [12] we know that the matrix around the rubber particle/void has actually undergone plastic deformation for the crack-tip stress system of $2.4\sigma_y : 1.7\sigma_y : 1.6\sigma_y$ because the maximum octahedral shear stress surpasses $0.47\sigma_y$. This result is also confirmed by the 3-D elastoplastic finite element analysis using the particle-crack tip interaction model. Hence the results from the Dewey's elastic solution [12] and the face-centred cuboidal cell model using *elastic* finite element analysis cannot give an accurate description of the actual stresses in the matrix and rubber particles ahead of a crack tip. On the other hand, the particle-crack tip interaction model can give the detailed stress distributions and the sequence of development the plastic zones very clearly. From Figs 8 and 9 we can see that the matrix surrounding the rubber particle/void undergoes plastic deformation before the crack-tip plastic zone arrives and then these two plastic regions are joined together.

To compare with the results obtained by Sue and Yee [12], we take the maximum octahedral shear stress, hydrostatic tension and principal stress normalised by the matrix yield strength for the particle-crack tip interaction model at $\bar{K}_I = 2.4$ when the matrix around the void is close to shear yielding but still deforms elastically. At this stage the principle stresses in the matrix around the rubber particle/void are lower than the principle stresses at the elastic-plastic boundary ($2.4\sigma_y : 1.7\sigma_y : 1.6\sigma_y$). Since the maximum stresses in the matrix around the rubber particle/void at the elastic stage increase nearly proportionally, we can compare the ratios of these maximum stresses for neat PC, PC/rubber and PC/void systems to assess the possibility of matrix crazing or shearing yielding as well as to understand the role of rubber cavitation in the toughening process.

From Table I we can see that maximum octahedral shear stress, hydrostatic tension and principal stress all decrease with increasing particle Poisson's ratio. There exists little difference in the stress concentrations around voids and around rubber particles with Poisson's ratio of 0.49 for all the cases studied. Stress

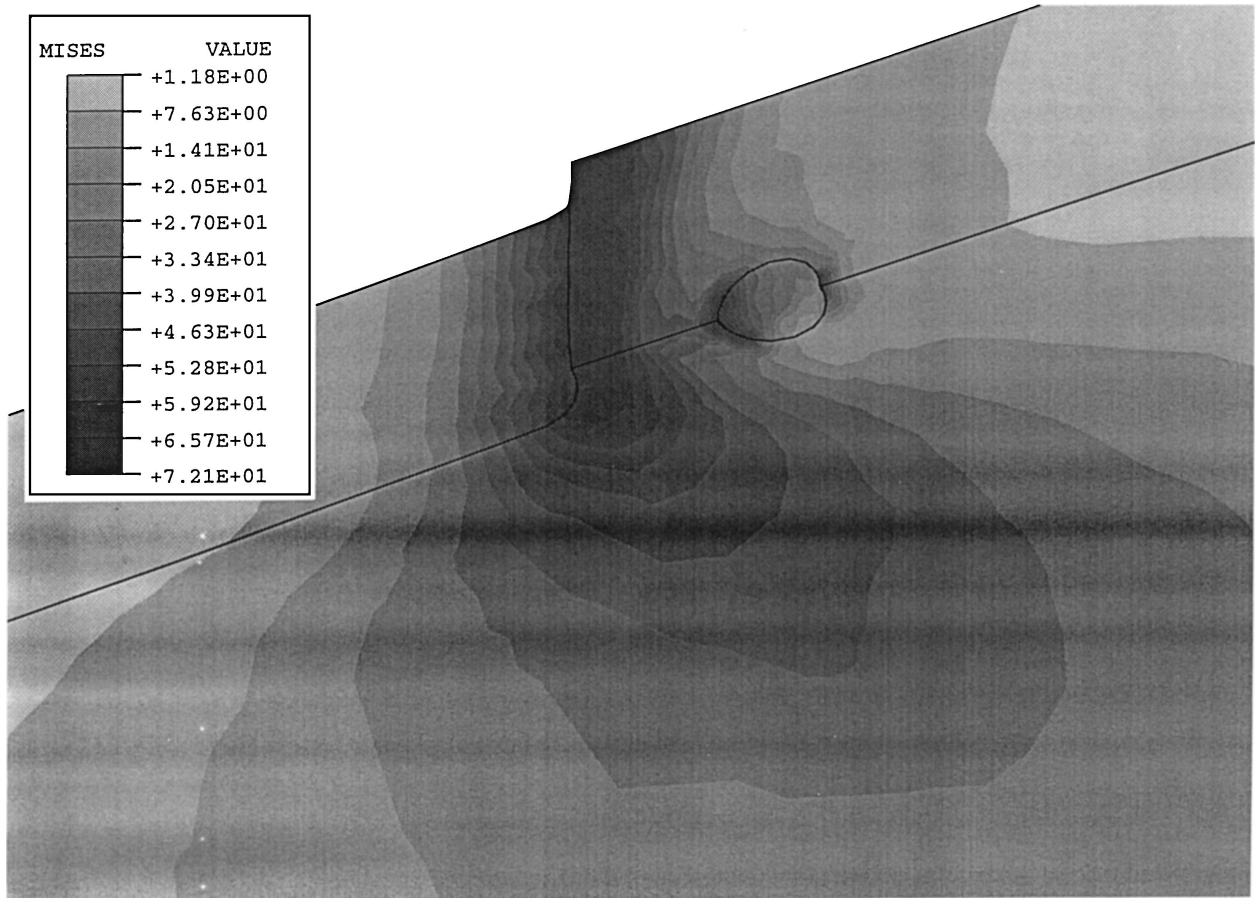

(a)

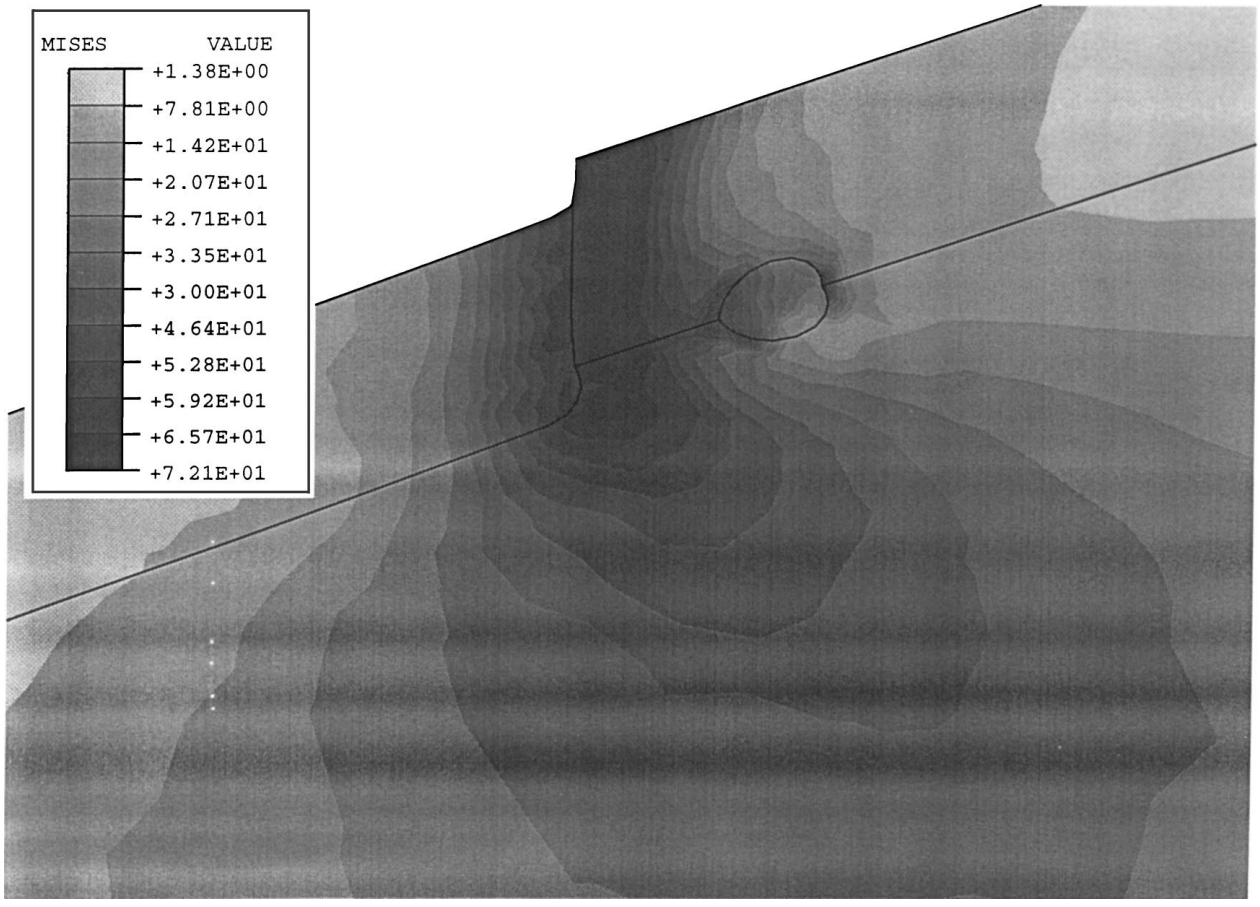

(b)

Figure 9 Contour plot of Von Mises stress in the central domain around the crack tip based on the deformed shape for void/crack tip system at a particle volume fraction of 1.68%: (a) $\bar{K}_I = 3.0$, (b) $\bar{K}_I = 3.4$, (c) $\bar{K}_I = 3.6$. (*Continued*).

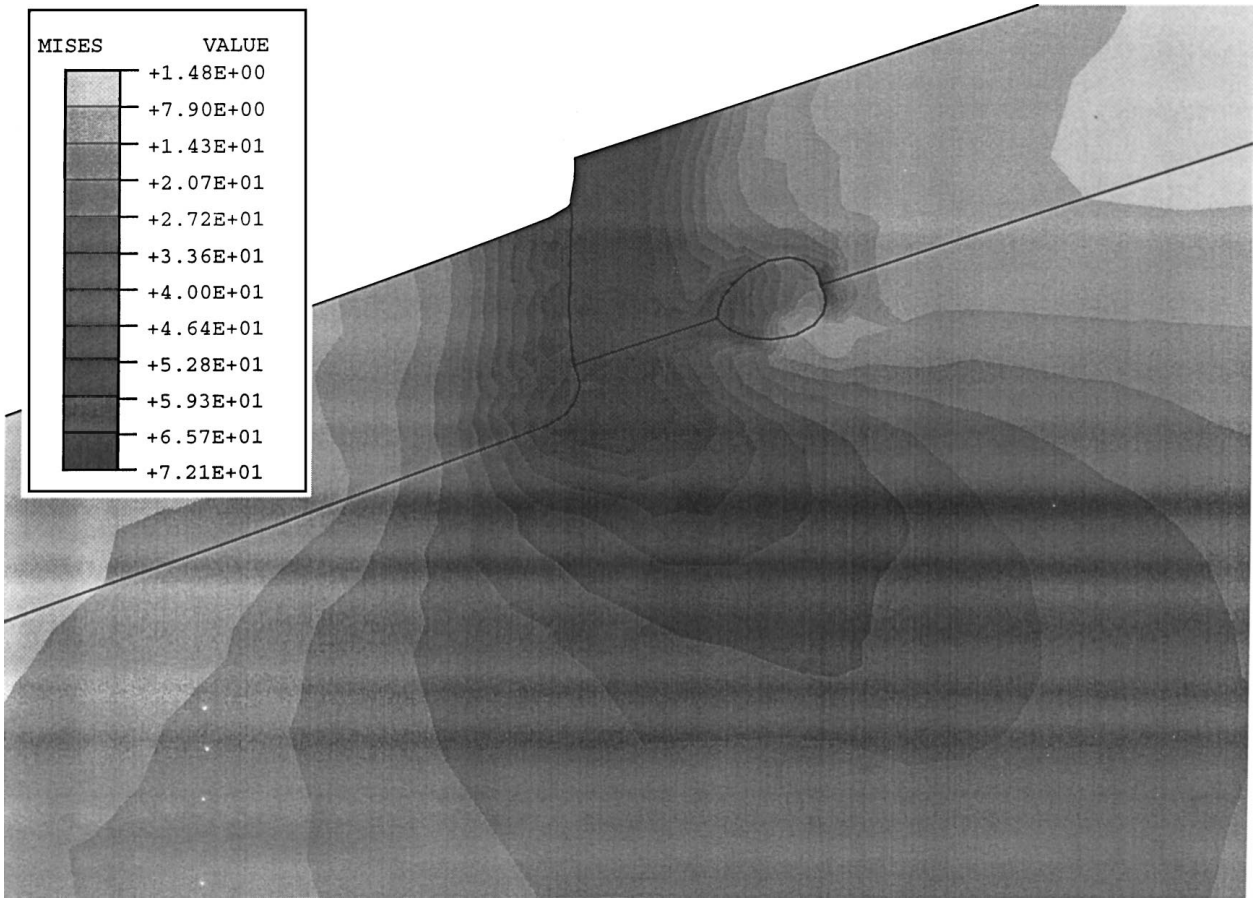

(c)

Figure 9 (*Continued*).

TABLE I Maximum octahedral shear stress (τ_{oct}), hydrostatic tension (p_{max}) and principal stress (σ_{max}) under various constraint /loading conditions

	τ_{oct}		p_{max}		σ_{max}	
	S & Y	This work	S & Y	This work	S & Y	This work
Cell model ($\sigma^e_{yy} : \sigma^e_{zz} : \sigma^e_{xx} = 1:0:0$)						
Neat PC	0.47	0.47	0.33	0.33	1.00	1.00
PC/rubber (0.4999)	—	0.79	—	0.85	—	1.93
PC/rubber (0.499)	0.79	0.87	0.82	0.91	1.92	2.12
PC/rubber (0.49)	—	0.89	—	0.93	—	2.18
PC/void	0.93	0.93	0.82	0.93	2.11	2.18
Cell model ($\sigma^e_{yy} : \sigma^e_{zz} : \sigma^e_{xx} = 2.4:1.7:1.6$)						
Neat PC	0.35	0.35	1.88	1.88	2.37	2.37
PC/rubber (0.4999)	—	0.80	—	2.32	—	3.11
PC/rubber (0.499)	0.70	1.47	2.28	2.53	2.98	4.06
PC/rubber (0.49)	—	1.64	—	2.62	—	4.25
PC/void	1.69	1.69	2.28	2.63	4.05	4.26
Particle-crack tip interaction model ($\bar{K}_I = 2.4$)						
Neat PC	—	0.087	—	0.64	—	0.76
PC/rubber (0.4999)	—	0.19	—	0.72	—	0.95
PC/rubber (0.499)	—	0.36	—	0.79	—	1.12
PC/rubber (0.49)	—	0.38	—	0.80	—	1.15
PC/void	—	0.40	—	0.80	—	1.16

concentrations drop quickly as particle Poisson's ratio exceeds 0.499, especially at high stress triaxiality. Good prediction of stress difference near the crack tip due to rubber cavitation can be given by the face-centred cuboidal cell model under the crack-tip stress system ($2.4\sigma_y : 1.7\sigma_y : 1.6\sigma_y$) rather than under uniaxial tension ($\sigma_y : 0 : 0$) in comparison with the particle-crack tip interaction model. For example, the ratio of maximum

octahedral shear stress around voids to that in neat PC is only 1.98 under uniaxial tension in contrast to 4.83 under the crack-tip stress system, which is similar to the prediction of 4.52 by the particle-crack tip interaction model. Maximum shear stress is predicted to increase more quickly than maximum hydrostatic tension and principal stress due to rubber cavitation near a crack tip by both the face-centred cuboidal cell model under a given crack-tip stress system and the particle-crack tip interaction model. The increasing ratios for maximum octahedral shear stress, principal stress and hydrostatic tension due to rubber cavitation at a rubber Poisson's ratio of 0.4999 are, respectively, 110, 23 and 11% by the particle-crack tip interaction model, and 111, 37 and 13% by the face-centred cuboidal cell model under the crack-tip stress system ($\sigma^{e}_{yy} : \sigma^{e}_{zz} : \sigma^{e}_{xx} = 2.4 : 1.7 : 1.6$). Hence rubber cavitation benefits matrix shear yielding more than matrix crazing. Our face-centred cuboidal cell model and Sue and Yee's model predict a similar general trend on the stress concentrations, however, it seems that their results for PC/rubber system with particle Poisson's ratio of 0.499 may be closer to our results for PC/rubber system with particle Poisson's ratio of 0.4999 instead of 0.499.

The dependence of hydrostatic tension at the centre of rubber particles and plastic strain in the mid-ligament between the crack tip and rubber particles on dimensionless stress intensity factor $\bar{K}_I$ at particle volume fractions of 1.68 and 13.40% is shown in Fig. 10. The path plots of plastic strain as a function of the distance from the crack tip for rubber/crack tip and void/crack tip systems at different $\bar{K}_I$ are shown in Figs 11 and 12 for particle volume fractions of 1.68 and 13.40%, respectively. The path is a straight line starting from the crack tip and passing the particle centre, which is the intersection of two symmetric planes of $y = 0$ and $z = a_0$.

We can see that both hydrostatic tension inside rubber particles and plastic strain in the ligament between the crack tip and rubber particles increase with decreasing inter-particle distance so that rubber cavitation and

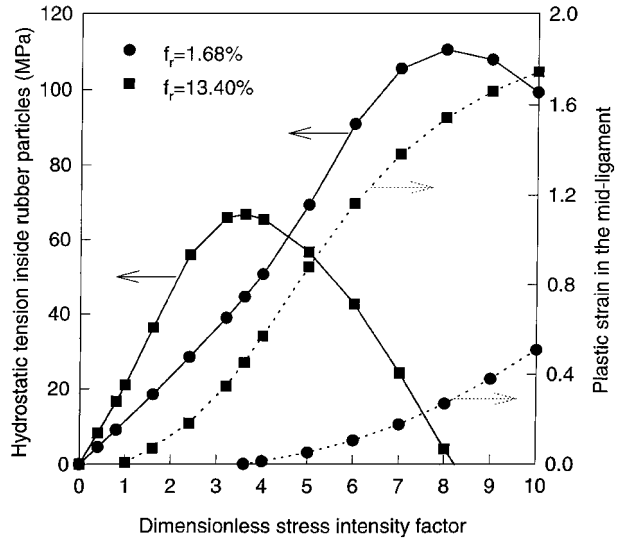

Figure 10 Dependence of hydrostatic tension at the centre of rubber particles and plastic strain in the mid-ligament on stress intensity factor at particle volume fractions of 1.68 and 13.40%.

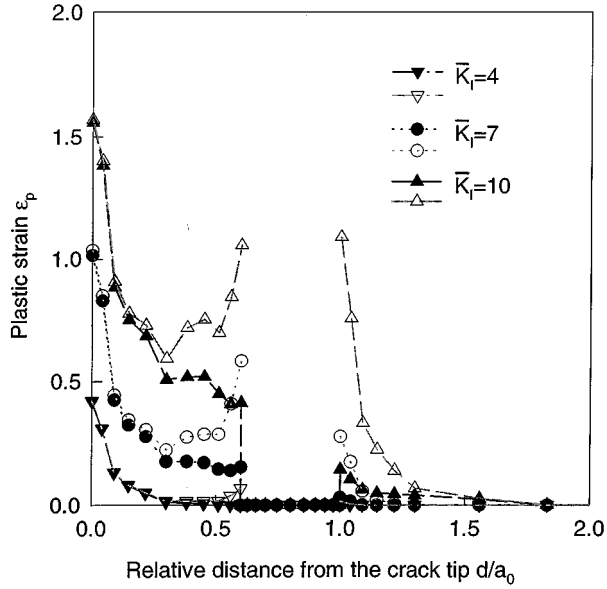

Figure 11 Plastic strain versus relative distance from the crack tip at different stress intensity factor for rubber particle/crack tip and void/crack tip systems at a particle volume fraction of 1.68%.

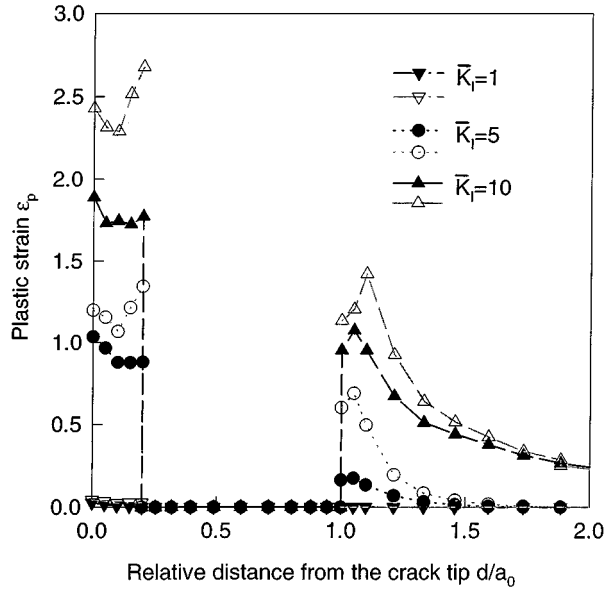

Figure 12 Plastic strain versus relative distance from the crack tip at different stress intensity factor for rubber particle/crack tip and void/crack tip systems at a particle volume fraction of 13.40%.

ligament shear yielding at a higher particle volume fraction can occur at a lower stress intensity factor. There exists a peak for the hydrostatic tension at the centre of rubber particles as the dimensionless stress intensity factor is around 3.6 and 8.0 for particle volume fractions of 13.40 and 1.68%, respectively. This trend was also obtained for the simple tension case by Schemer *et al.* [10] with their two-dimensional plane-strain finite element model. Rubber cavitation must occur before the hydrostatic tension reaches the maximum value.

If cavitation strength for rubber particles is within the range of 8 to 20 MPa, rubber particles can easily cavitate before shear yielding occurs in the surrounding matrix, which is consistent with the experimental observation by Parker *et al.* [6]. For example, hydrostatic tension at the centre of rubber particles reaches 9.14,

18.48 and 28.37 MPa at $\bar{K}_I = 0.8, 1.6$ and 2.4 for a particle volume fraction of 1.68% in comparison with 8.28, 16.64 and 21.05 MPa at $\bar{K}_I = 0.4, 0.8$ and 1.0 for a particle volume fraction of 13.40%.

Plastic deformation grows more quickly with increasing $\bar{K}_I$ in void/crack tip system than in rubber/crack tip system. Plastic strain around rubber particles at a particle volume fraction of 1.68% is 0.23% and 41.34% at $\bar{K}_I = 4$ and $\bar{K}_I = 10$ in comparison with 6.75% and 105.7% around voids. Therefore, undamaged rubber particles in the triaxial tension area have strong constraint effects on plastic deformation of surrounding matrix due to their high bulk modulus.

4. Conclusions

Our three-dimensional elastoplastic finite element modelling of deformation and fracture behaviour of rubber-modified PC is compatible with experimental observations by Yee and coworkers [5, 6] and Wu and Mai [7]. That is, rubber particles can act as stress concentrators to initiate crazing or shear yielding in the matrix but they behave quite differently from voids at high triaxiality due to their high bulk modulus which enables them to maintain the triaxial constraint. Rubber particles sustain hydrostatic tension high enough to cavitate prior to matrix shear yielding so that extensive plastic deformation can be developed in the matrix. Effective elastic moduli decrease with increasing rubber volume fraction. The dependency is closer to the prediction by the Mori-Tanaka theory than by the Voigt's upper bound. Effective yield behaviour depends greatly on the hydrostatic stress and particle volume fraction. Both hydrostatic tension inside rubber particles and plastic strain in the ligament between the crack tip and rubber particles increase with decreasing inter-particle distance. The higher the particle volume fraction, the lower the stress intensity factor required for rubber cavitation and ligament shear yielding. There may be an optimum particle volume fraction for the enhancement of fracture toughness because of the increased propensity to shear yielding but a reduction in the load carrying capacity at a higher particle volume fraction. Maximum shear stress, hydrostatic tension and principal stress all increase with decreasing particle bulk modulus. Subsequent to rubber cavitation maximum shear stress increases much more quickly than maximum hydrostatic tension and principal stress. Rubber cavitation, therefore, favours matrix shear yielding more than matrix crazing. The big stress difference between rubber/crack tip and void/crack tip systems can be predicted well by the face-centred cuboidal cell model under a given crack-tip stress system rather than under uniaxial tension when compared with the particle-crack tip interaction model. The particle-crack tip interaction model is essential to provide a clear picture of the stress distribution around the crack tip and rubber particles/voids and the sequence of matters.

Acknowledgements

The authors wish to thank the Australian Research Council (ARC) for the continuing support of the polymer blends project. XH Chen is grateful for an ARC Postdoctoral Fellowship.

References

1. C. B. BUCKNALL, "Toughened Plastics" (Applied Science Publisher Ltd., London, 1977).
2. A. C. GARG and Y.-W. MAI, *Comp. Sci. and Technol.* **31** (1988) 179.
3. C. K. RIEW and A. J. KINLOCH, "Toughened Plastics I," Advances in Chemistry Series 233 (American Chemical Society, Washington, DC, 1993).
4. *Idem.*, "Toughened Plastics II," Advances in Chemistry Series 252 (American Chemical Society, Washington, DC, 1996).
5. A. F. YEE and R. A. PEARSON, *J. Mater. Sci.* **21** (1986) 2462.
6. D. S. PARKER, H.-J. SUE, J. HUANG and A. F. YEE, *Polymer* **31** (1990) 2267.
7. J. S. WU and Y.-W. MAI, *J. Mater. Sci.* **28** (1993) 6167.
8. H.-J. SUE and A. F. YEE, *Polymer* **29** (1988) 1619.
9. Y. HUANG and A. J. KINLOCH, *J. Mater. Sci.* **27** (1992) 2753, 2763.
10. B. SCHEMER, T. KURIYAMA, I. NARISAWA and K. Friedrich, *J. Mater. Sci. Lett.* **14** (1995) 660.
11. F. J. GUILD and A. J. KINLOCH, *J. Mater. Sci.* **30** (1995) 1689.
12. H. -J. SUE and A. F. YEE, *Polym. Eng. Sci.* **36** (1996) 2320.
13. X.-H. CHEN and Y.-W. MAI, *Key Eng. Mater.* **137** (1998) 115.
14. *Idem., J. Mater. Sci.* **33** (1998) 3529.
15. Y. S. WU, J. S. WU and Y.-W. MAI, in Proc. Materials Research 96, Vol. 1 (IMMA, Queensland, July 1996) p. 153.
16. *Idem.*, in "Fatigue and Fracture Mechanics," Vol. 28, ASTM STP 1321, edited by J. H. Underwood, B. D. MacDonald and M. R. Mitchell (American Society for Testing and Materials, Conshohocken, PA, USA, 1997) p. 671.
17. C. L. HOM and R. M. MCMEEKING, *J. Appl. Mech.* **56** (1989) 309.
18. *Idem., International Journal of Fracture* **42** (1990) 1.
19. A. LASSERI and C. B. BUCKNALL, *J. Mater. Sci.* **28** (1993) 6799.
20. J. F. KNOTT, "Fundamentals of Fracture Mechanics" (John Wiley & Sons, New York, 1976).
21. J. ABOUDI, "Mechanics of Composite Materials" (Elsevier, Amsterdam, 1991) chap. 2.

Received 29 July
and accepted 11 November 1998